Journal of Sound and Vibration 329 (2010) 848–865

Contents lists available at ScienceDirect

Journal of Sound and Vibration

journal homepage: www.elsevier.com/locate/jsvi

Non-modal dynamics before flow-induced instability in fluid–structure interactions

G. Coppola [a,*], L. de Luca [b]

[a] DETEC, Università degli studi di Napoli "Federico II", Italy
[b] DIAS, Università degli studi di Napoli "Federico II", Italy

ARTICLE INFO

Article history:
Received 23 December 2008
Received in revised form
7 October 2009
Accepted 7 October 2009
Handling Editor: C.L. Morfey
Available online 30 October 2009

ABSTRACT

A theoretical investigation of the subcritical dynamics of typical fluid–structure interactions is carried out by applying the linear non-modal operators theory combined with direct numerical simulations. The cases of thin panel exposed to subsonic and supersonic fluid flows and pipe conveying a fluid are considered. In order to make the problem tractable for the rather wide range of cases, simple pressure models are employed, where the relevant instability is essentially of modal-coalescence type. Transient energy amplifications, here termed *optimal* and *global*, are found, which exhibit low-frequency oscillations corresponding to the continuous extraction/release of energy from/to the fluid. The low frequency is always related to the spacing between the imaginary parts of the coupling eigenvalues, which represent essentially the non-normal part of the spectrum. This suggests that the periodic transfers of energy along the route to the instability can be predicted by a simple model of damped forced vibrations. Although the major findings are obtained with crude pressure models, the authors' opinion is that most of the effects discussed in the paper should survive to the use of flow dynamics modeling based on full Navier–Stokes equations, at least at high Reynolds number flows.

1. Introduction

Flutter and divergence instabilities of a thin streamlined and deformable body interacting with a fluid current are a physical phenomenon commonly observed in a variety of science and engineering situations. In spite of the remarkable bulk of modern papers, these instabilities and the related flow-induced flapping dynamics do not seem exhaustively studied under all their aspects. It is well known that under certain circumstances the system can lose its stability, which occurs in both supersonic and subsonic flows. Linear analysis shows that the instability is associated to a variety of spectrum morphologies, depending on how eigenvalues cross the stability margin in the complex frequency-plane (for a recent comprehensive review see for example Païdoussis [1,2]).

For plates in axial flow the basic control parameters usually employed are the density ratio $\mu = \rho_\infty L/\rho_s h$, which characterizes the added mass effect, ρ_∞ and ρ_s being the fluid density and that of the panel (of length L and thickness h), respectively, and the velocity ratio V of the fluid velocity V_∞ to the velocity of the so-called bending waves V_B. Typically, for a fixed μ the instability is seen to emerge with increasing the velocity ratio, and similar occurrences are encountered in other fluid–structure interactions such as the fluid-conveying pipe model.

* Corresponding author.
E-mail address: gcoppola@unina.it (G. Coppola).

0022-460X/$ - see front matter © 2009 Elsevier Ltd. All rights reserved.
doi:10.1016/j.jsv.2009.10.010

For thin plates in axial flow the theories and the applications developed in the literature employ a variety of analytical models and numerical tools. Models have mainly been developed by considering linear beam theory for the structure and potential flow for the external aerodynamics. In subsonic flow one encounters various approximations, ranging from Theodorsen-like models [3–6] to unsteady vortex models [7–9]. For supersonic flow, the external flow is still usually treated as potential, with occasional corrections arising from the boundary layer influence. Early reviews of the subject are due to Dowell et al. [10] and Dugundji [11] and a special mention of the monograph of Dowell [12] is deserved. This list of papers is largely incomplete because the literature is quite huge and it is still growing. The fluid-conveying pipe problem is a huge topic too, mainly because of its prototypical character [13].

Generally speaking, the previous papers deal with both the conditions leading to the instability and the post-critical behavior. Some unresolved issues still remain, the most notably one being the subcritical bifurcation of soft panels in subsonic flow, with the formation of a hysteresis loop [14,15,9]. Among more recent contributions, Abrahams and Wickham [16] and Pitman and Lucey [17] analyzed the effect of the structural damping and showed that it changes remarkably the instability characteristics. The former authors studied the damping influence on the absolute/convective nature of the instability, the latter showed that for damped plates the divergence merges into flutter instability with increasing the dimensionless velocity parameter. Howell et al. [18] carried out direct numerical simulations of the behavior of a cantilevered-free plate and found time oscillations of the plate energy by monitoring crucial energy transfers between fluid and structure. These last findings are reminiscent of a similar oscillatory behavior which will be discussed in the central body of the present paper. Nonetheless, they are of different nature, the major reason being that the energy oscillations of Howell et al. [18] are linked to the classical *local* flapping dynamics, whereas present results refer to *global* oscillations, where the term *global* here means that the fluctuations concern the *entire* structure.

The present contribution starts from a quite different perspective, inspired by the not yet investigated non-normal character of the typical partial differential equation of motion. It is widely recognized that in the field of the hydrodynamic stability of shear flows, non-normal features of the operator governing the linear evolution of disturbances strongly modified the findings based on the eigenvalue analysis. The present paper aims to address the nature of the subcritical (i.e. before the occurrence of instability) linear non-modal dynamics of some fluid–structure interactions, here seen as prototypical, representing a novelty in this subject. Within this context a relatively recent paper of Schmid and de Langre [19] is our starting point. It analyzes the occurrence of global transient growth of energy before the onset of couple-mode flutter by restricting the analysis to simple two degrees-of-freedom finite-dimensional models derived by classical problems. They were able to show that the energy of such systems may grow by a factor of more than 10 before the threshold of flutter is crossed, and some later experimental results on the stability of rigid wing configurations seem to corroborate such findings [20]. However, the survival of such effects in the continuum limit and their extension to more realistic models of deformable structures have not been investigated. This lack is the motivating reason of the present paper.

With reference to typical forms of the equation of motion governing the dynamics of thin elastic panels and fluid-conveying pipes, it will be shown that subcritical global amplifications of energy occur and quantitative results will be shown. Furthermore, the transient energy growth of disturbances exhibits significant time-periodic oscillations. The period of such oscillations is not related to the frequency of flapping at critical conditions, as in the paper of Howell et al. [18], whilst it is always related to the morphology of the spectrum (as already showed for convection-driven models by Coppola and de Luca [21]). More specifically, we will see that the global oscillatory behavior is of low-frequency, as opposed to the more standard local one which is of high-frequency. The non-modal analysis will be combined with a numerical simulation of the dynamic behavior of the system. It is worth pointing out that while the direct numerical simulation solves an initial-value problem, the non-modal analysis yields the maximum energy amplification over all possible initial conditions, in fact its output is usually termed *optimal*. Readers have to be made fully aware that, in order to make the problem tractable in a wide variety of cases, rather crude closed-form pressure models are considered. These models generally lead to modal-coalescence instability. In the opinion of the authors the core of the present results should survive in more complex cases of higher-order single-mode flutter and numerical modeling of the flow dynamics based on full Navier–Stokes equations is strongly recommended for advanced calculations. This issue will be briefly discussed in the conclusions.

The paper is organized as follows. In Section 2 the basic equation is presented and the connections between the present model and the finite-dimensional model of Schmid and de Langre [19] are highlighted. In Section 3 the fundamentals of non-modal analysis are recalled and the numerical procedure employed is described. Section 4 is devoted to the results, detailed for the various situations and for the different pressure models employed. In Section 5 some conclusions are finally drawn.

2. Modeling

The model equation used here to study the behavior of a streamlined body interacting with a fluid flow is

$$m\frac{\partial^2 Y}{\partial \tau^2} = -B\frac{\partial^4 Y}{\partial X^4} - \Delta P - D\frac{\partial Y}{\partial \tau} \tag{1}$$

where inertia, bending elasticity, aerodynamic pressure and structural damping are included. X and Y are the axial spatial coordinate and the transverse deflection, respectively, and τ is time. For the case of a plate in axial flow m is equal to $\rho_s h$,

while for a pipe conveying fluid it is the mass per unit length of the pipe. B is the flexural rigidity and ΔP is the forcing pressure arising from the interaction with the fluid, namely the pressure difference between upper and lower surfaces for the plate and the pressure variation related to the fluid acceleration for the pipe. D is the damping coefficient. Occasionally some other terms may be included, such as the shear flow induced tension and the effects of an elastic foundation.

Eq. (1) may be conveniently recast in a non-dimensional form. In the case of plate we define $x = X/L$, $y = Y/L$, $t = \tau/t_r$ with $t_r = L^2/\sqrt{B/(\rho_s h)}$, $V = V_\infty/V_B$ with $V_B = \sqrt{B/(\rho_s h)}/L$, $p = \Delta P/(\rho_\infty V_\infty^2)$, and $d = L^2 D/\sqrt{\rho_s h B}$. These definitions lead to the following equation, where the two dimensionless parameters μ and V have been already defined:

$$\frac{\partial^2 y}{\partial t^2} = -\frac{\partial^4 y}{\partial x^4} - \mu V^2 p - d\frac{\partial y}{\partial t} \tag{2}$$

The above model agrees with most models presented in a consistent body of literature. In the case of pipe, a slightly different choice of the characteristic quantities is usually employed. Following Païdoussis [1,13] the characteristic time is $t_r = L^2/\sqrt{B/(M+m)}$, where M is the fluid mass per unit length. The corresponding dimensionless groups are: $\beta = M/(M+m)$ and $u = UL\sqrt{M/B}$, where U is the (constant) velocity of the fluid inside the pipe. The complete dimensionless form of the equation of motion is reported in Section 4.5 after deriving a suitable expression of the pressure term ΔP.

The boundary conditions for the equation of motion explored in this paper refer to clamped–clamped, pinned–pinned and clamped–free configurations. They read

$$y(0) = \frac{\partial y}{\partial x}(0) = 0 \quad \text{and} \quad y(1) = \frac{\partial y}{\partial x}(1) = 0, \quad \text{C}-\text{C} \tag{3}$$

$$y(0) = \frac{\partial^2 y}{\partial x^2}(0) = 0 \quad \text{and} \quad y(1) = \frac{\partial^2 y}{\partial x^2}(1) = 0, \quad \text{P}-\text{P} \tag{4}$$

$$y(0) = \frac{\partial y}{\partial x}(0) = 0 \quad \text{and} \quad \frac{\partial^2 y}{\partial x^2}(1) = \frac{\partial^3 y}{\partial x^3}(1) = 0, \quad \text{C}-\text{F} \tag{5}$$

Before performing a detailed analysis of the non-normal characteristics of such a model problem, it has to be stressed that Eq. (2) cannot be considered as the continuous counterpart of the two-degrees-of-freedom model studied by Schmid and de Langre [19]. In fact, the present authors extended that model to a generic number N of degrees-of-freedom, $N>2$, and they found (this argument is physically deducible and will not be formally developed in the present paper) that it is not consistent for $N\to\infty$ with the continuous model of the dynamics of an inextensible two-dimensional plate, namely Eq. (1), without structural damping. On the contrary, consistency is achieved with a model of N lumped masses whose equations of motion are derived by means of the method of the influence coefficients, which are determined through the flexural deflection of the (massless) panel divided into $N+1$ elements. In the case of two-degrees-of-freedom, when the pressure field is of the steady supersonic kind and given by $\Delta P = (\rho_\infty V_\infty^2/M_\infty)(\mathrm{d}Y/\mathrm{d}X)$ [12], for the pinned–pinned case the influence coefficients model writes

$$\begin{aligned} \alpha_{11}\ddot{y}_1 + \alpha_{12}\ddot{y}_2 + 2\cdot 3^3 y_1 &= -2\lambda(\alpha_{11}y_1 - \alpha_{12}y_2) \\ \alpha_{21}\ddot{y}_1 + \alpha_{22}\ddot{y}_2 + 2\cdot 3^3 y_2 &= -2\lambda(\alpha_{21}y_2 - \alpha_{22}y_1) \end{aligned} \tag{6}$$

where $\lambda = \rho_\infty V_\infty^2/(2M_\infty k)$ is the coupling parameter formally identical to the definition given by Dowell et al. [12], M_∞ is the flow Mach number and the spring constant k here is substituted by B/L^3. The coefficients of the influence matrix are $\alpha_{11} = \alpha_{22} = \frac{4}{9}$ and $\alpha_{12} = \alpha_{21} = \frac{7}{18}$. Double dots stand for the second derivative of the relevant quantities with respect to time.

However, the mathematical structure of Eqs. (6) is equivalent to that proposed by Dowell et al. [12] (on which Schmid and de Langre [19] carried out their non-normality analysis) and mimics the dynamics of two coupled oscillators:

$$\begin{aligned} \ddot{q}_1 + \Omega_1^2 q_1 &= caq_2 \\ \ddot{q}_2 + \Omega_2^2 q_2 &= -aq_1 \end{aligned} \tag{7}$$

where q_1 and q_2 are the generalized coordinates $q_1 = y_1 + y_2$ and $q_2 = y_1 - y_2$, $a = 2\lambda$ is the coupling parameter, Ω_1 and Ω_2 are the frequencies of the free oscillators, c is an additional parameter. Eqs. (6) may be easily transformed to the form (7) with $\Omega_1 = 8.05$, $\Omega_2 = 31.18$, $c = 1$. It should be noted that for pinned–pinned end conditions the two exact lowest natural frequencies are 9.87 and 39.48. A better approximation is of course attained by increasing the number of masses. Schmid and de Langre [19] showed that the dynamics of two coupled oscillators is non-modal in subcritical conditions, i.e. when

$$a < \frac{\Omega_1^2 - \Omega_2^2}{2\sqrt{c}}$$

Thus, we postulate the existence of optimal transient growths of energy for the continuous model starting from the consideration that the same non-normal properties are exhibited by the consistent finite-dimensional model.

3. Numerical treatment

3.1. Spectral analysis

By introducing the variables transformation (subscript denotes differentiation):

$$f = y, \quad g = y_t$$

Eq. (2) can be recast in the following form:

$$\begin{cases} f_t = g \\ g_t = -f_{xxxx} - \mathcal{P}(f,g) - dg \end{cases} \tag{8}$$

where $\mathcal{P}$ is a linear operator expressing the pressure action in terms of the displacement variable and of its time derivative. The assumption of exponential time dependence for the variables f and g: $f = \tilde{f}(x)e^{\omega t}$, $g = \tilde{g}(x)e^{\omega t}$ leads to an eigenvalue problem which can be expressed in matrix form as follows:

$$\omega \begin{pmatrix} \tilde{f} \\ \tilde{g} \end{pmatrix} = \left(\begin{array}{c|c} \mathcal{O} & \mathcal{I} \\ \hline -\mathcal{D}^4 + \mathcal{A} & \mathcal{B} \end{array}\right) \begin{pmatrix} \tilde{f} \\ \tilde{g} \end{pmatrix} \tag{9}$$

where $\mathcal{O}$, $\mathcal{I}$, and $\mathcal{D}^4$ denote the null, identity and fourth-order spatial derivative operators, respectively, $\mathcal{A}$ and $\mathcal{B}$ are the operators in which $\mathcal{P}$ decomposes, and each couple of functions $(\tilde{f},\tilde{g})^{\mathrm{T}}$ satisfying (9) is an eigenfunction of the problem associated to the eigenvalue ω. The eigenvalue problem (9) is posed on the normalized domain [0, 1]. The four boundary conditions required are given by one of the sets:

$$\tilde{f}(0) = \tilde{f}(1) = \tilde{f}_x(0) = \tilde{f}_x(1) = 0$$

$$\tilde{f}(0) = \tilde{f}(1) = \tilde{f}_{xx}(0) = \tilde{f}_{xx}(1) = 0$$

$$\tilde{f}(0) = \tilde{f}_x(0) = \tilde{f}_{xx}(1) = \tilde{f}_{xxx}(1) = 0$$

respectively, for pinned–pinned, clamped–clamped and clamped–free configurations. The same conditions of course hold for the velocity eigenfunction $\tilde{g}$.

The eigenvalue problem (9) has been solved by adopting a Chebyschev collocation spectral method, which is particularly suited for eigenvalue problems [22,23]. In order to perform the discretization, the integration domain [0, 1] is firstly mapped to the Chebyshev domain $[-1,1]$ by means of a simple linear transformation. The eigenfunctions are then expanded in a series of $N+1$ Chebyshev polynomials and introduced into Eq. (9), and the condition of null residual is imposed at the Chebyshev–Lobatto points. This procedure leads to a discretized eigenvalue problem of order $2(N+1)$ which is solved by means of a global eigenvalue method. In order to discard the spurious and non-physically relevant eigenvalues produced by this technique, an individual convergence check for each eigenvalue is needed. The computations are performed by taking advantage of the DMSUITE package of Weideman and Reddy [24]. Boundary conditions are implemented by replacing rows, following the technique illustrated in that paper. Numerical linear algebra computations are performed in MATLAB.

The numerical simulations shown below have been performed by using the same spatial discretization employed in the spectral analysis and an implicit Euler backward formula for temporal discretization. A satisfying accuracy is achieved with maximum N values of order 100.

3.2. Non-modal analysis

It has been widely recognized that when an operator is non-normal (i.e. when the eigenfunction basis is not orthogonal) inferring the stability of the system by employing normal modes alone may be misleading. In non-normal systems the components of the solution to the governing equation in the eigenfunctions basis can be greater than the norm of solution. Even though in an asymptotically stable system all the exponential terms decay, for moderate time scales the large components, which cancel at $t = 0$, survive because the initial cancelation generally does not occur. Therefore, asymptotically stable systems can exhibit solutions whose norm experiences high amplifications (larger than its initial value) on a short time scale and non-linearities can be triggered, which eventually make the system unstable. The non-modal theory is not used here in order to try to infer conclusions on the presence of subcritical instabilities, they should exist. On the contrary, we wish to emphasize its major effects on the subcritical dynamics, and to describe some important related physical mechanisms.

In the following we will quickly present some standard tools for the analysis of non-normal operators governing initial value problems. For a more comprehensive review the reader is referred to Schmid and Henningson [25] and Trefethen and Embree [26].

The initial-boundary value problem under consideration can be recast in the form of a linear evolution process on its underlying Hilbert space. To this end the system (8) is rewrited conveniently as

$$\varphi_t = \mathcal{L}\varphi \tag{10}$$

where the vector function $\varphi = (f, g)$ satisfies the prescribed boundary conditions and $\mathcal{L}$ is the operator within round brackets of Eq. (9). In order to measure the energy of the plate, we define at first the scalar product:

$$(\varphi_1, \varphi_2)_E = \int_0^1 (f_{2xx}^* f_{1xx} + g_2^* g_1)\,\mathrm{d}x$$

where * denotes complex conjugate quantity and φ_1 and φ_2 are any two elements of the relevant Hilbert space. The squared norm of a solution accordingly yields the structure disturbance energy (we are not including the energy associated to disturbances in the fluid):

$$E_{\mathrm{tot}} = \frac{1}{2}\|\varphi\|_E^2 = \frac{1}{2}\int_0^1 (f_{xx}^2 + g^2)\,\mathrm{d}x = \frac{1}{2}\int_0^1 (y_{xx}^2 + y_t^2)\,\mathrm{d}x \tag{11}$$

where the first and second terms in the integrals refer, respectively, to the potential and kinetic energy contributions. An energy balance yields the temporal variation of the energy norm:

$$\frac{\mathrm{d}E_{\mathrm{tot}}}{\mathrm{d}t} = -\int_0^1 p y_t\,\mathrm{d}x - d\int_0^1 y_t^2\,\mathrm{d}x \tag{12}$$

where the two right-hand side terms represent the work per unit time performed by the fluid pressure (i.e. the energy exchange rate between fluid and structure $Q_e = -\int_0^1 p y_t\,\mathrm{d}x$) and the energy dissipation rate due to the structural damping within the system, respectively. It is worth noting that the rate of work is not defined in signum (as opposed to the corresponding damping term), hence a growth in energy can occur even for asymptotically stable and damped systems. In order to collect into a single function the effects of such exchanges of energy between fluid and structure, regardless of the initial condition, it is convenient to define a growth function $G(t)$ as

$$G(t) = \sup_{\varphi(x,0)\neq 0} \frac{\|\varphi(x,t)\|_E^2}{\|\varphi(x,0)\|_E^2} = \|\mathrm{e}^{\mathcal{L}t}\|_E^2$$

For each current time t, it represents the greatest possible amplification in energy of an initial perturbation and it is hence the envelope of the energy evolution of all initial conditions with unit norm. The initial condition which attains the maximum gain is usually termed *optimal perturbation*. A procedure to calculate $G(t)$ is described by Reddy and Henningson [27].

4. Results

4.1. Supersonic panel flutter

Let us first consider the case of a panel subjected to a supersonic pressure field. Following Dowell [12], for high supersonic Mach numbers ($M_\infty > 1.7$) the aerodynamic pressure can be described with the "piston theory" approximation:

$$\Delta P = \frac{\rho_\infty V_\infty^2}{M_\infty}\left(\frac{\partial Y}{\partial X} + \frac{1}{V_\infty}\frac{\partial Y}{\partial \tau}\right)$$

After reduction to dimensionless form and substitution into Eq. (2) one gets

$$\frac{\partial^2 y}{\partial t^2} = -\frac{\partial^4 y}{\partial x^4} - \frac{\mu V^2}{M_\infty}\frac{\partial y}{\partial x} - \frac{\mu V}{M_\infty}\frac{\partial y}{\partial t}$$

where no structural damping is taken into account. Following various authors it is convenient to introduce the parameter $\lambda^2 = \mu V^2$ so as to rewrite

$$\frac{\partial^2 y}{\partial t^2} = -\frac{\partial^4 y}{\partial x^4} - \lambda^2\frac{\partial y}{\partial x} - \lambda\sqrt{\mu}\frac{\partial y}{\partial t} \tag{13}$$

where for the sake of simplicity we set $M_\infty = 1$. For any actual Mach number the effective control parameters should be scaled as $\lambda_{\mathrm{eff}} = \lambda\sqrt{M_\infty}$ and $\mu_{\mathrm{eff}} = \mu M_\infty$.

At higher Mach numbers, under the assumption of *low frequency* conditions, the unsteady term (the so-called aerodynamic damping) can be neglected and then the pressure term becomes proportional to the local slope of the panel. It is worth noting that in this simplified case the only control parameter is λ and Eq. (13) becomes exactly the continuous counterpart of system (6), that is to say of Eqs. (7) with $c = 1$. The boundary conditions here analyzed are of pinned–pinned type (Eqs. (4)).

The dynamics of the morphology of the spectrum as the parameter λ is increased from the null value is well documented in the literature [11,12]: in absence of damping, starting from the *in vacuo* situation, for relatively small values of λ the spectrum lies on the imaginary axis; as λ increases the first two eigenvalues (the ones with the smallest

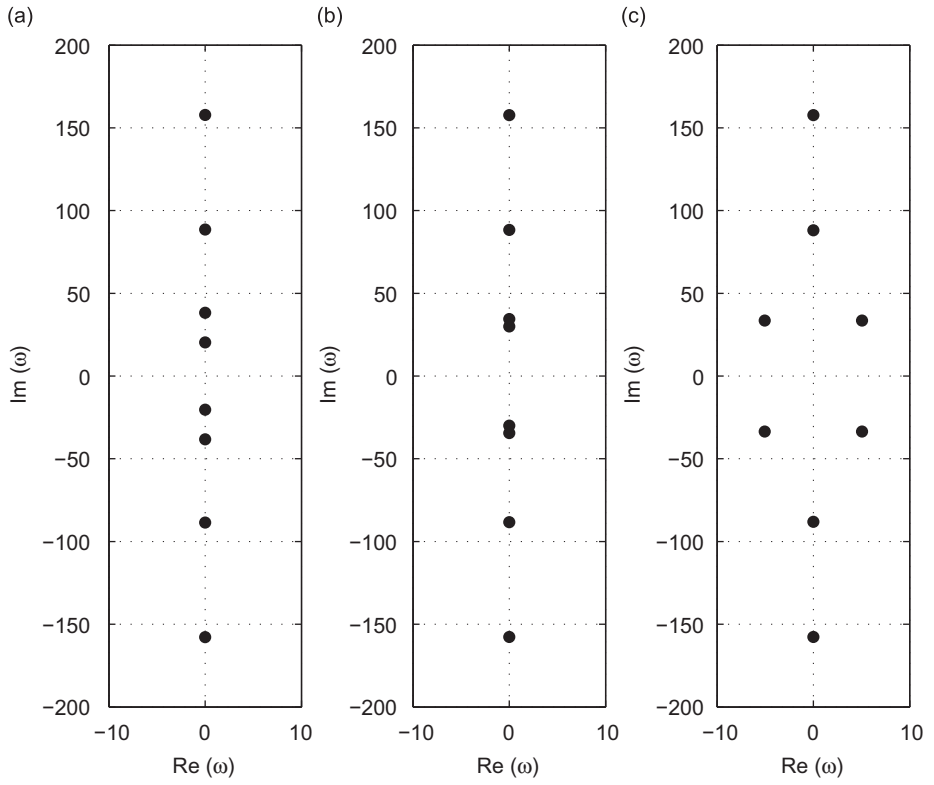

Fig. 1. Spectra for the model of the plate in supersonic flow, Eq. (13) with no flow-induced damping. Values of λ^2/λ_{cr}^2: (a) 0.7, (b) 0.98, (c) 1.1, pinned–pinned case.

frequencies) move toward each other and when it finally equals a certain critical value λ_{cr} (here $\lambda_{cr} \simeq 18.53$), they collide and subsequently split, moving in opposite directions in the stable and unstable regions of the complex plane, giving rise to the coupled-mode flutter instability. Fig. 1 depicts the relevant part of the spectrum for three values of the parameter λ^2/λ_{cr}^2. Imaginary parts of the first four eigenfunctions (displacement variable) are reported in Fig. 2. These plots show that while the first two eigenfunctions lose their symmetry as the coupling parameter increases, approaching the same shape at the critical value, the other eigenfunctions are only slightly affected by the coupling parameter. Note that the critical non-dimensional flutter frequency is $\mathrm{Im}(\omega_1) = \mathrm{Im}(\omega_2) = 32.43$. It is also interesting to observe that the third eigenvalue ω_3 is practically unaffected by the pressure forcing, resulting $\mathrm{Im}(\omega_3) = \pm 88.83$ in the absence of coupling and $\mathrm{Im}(\omega_3) = \pm 88.26$ at critical conditions.

Hence, in subcritical conditions the first two eigenmodes become progressively far from orthogonal as the forcing parameter increases, until they coincide. This implies that a generic disturbance having a non-null projection on the subspace spanned by these two modes can experience a transient growth in subcritical conditions. These arguments could be made more quantitative by the use of some other tools not presented here (namely pseudospectra and numerical range), however, they are directly confirmed by the time trend of the growth function depicted in Fig. 3, where optimal growths of energy up to values of thousands are evident.

A major feature of the growth function $G(t)$ is its oscillatory behavior which is not linked either to the flutter frequency or to one of the two frequencies moving in subcritical conditions. The period of the oscillations is growing with λ, approaching infinity as the critical conditions are reached, no damping effect being considered. According to a previous result of Coppola and de Luca [21], this period is strictly linked to the spacing $\Delta\omega$ between the imaginary parts of the first two eigenvalues, $T = 2\pi/\Delta\omega$. From the physical viewpoint, as will become clearer from the numerical simulations shown hereafter, the plate is able to extract/release energy from/to the flow in a periodic fashion, with a frequency smaller than the critical flapping frequency. This finding substantiates the picture that the route to panel instability is represented, for the present case under examination, by an oscillatory low frequency transfer of energy having period and amplitude progressively increasing as the critical condition is approached. The low-frequency oscillations have been termed *global* in the introduction section because they refer to the entire structure as a whole.

In order to sum up the results, the maximum value of G for all time, G_{max}, is reported in Fig. 4 as a function of λ^2/λ_{cr}^2 for the supersonic steady model equipped with various boundary conditions as well as for the subsonic clamped–free model of Argentina and Mahadevan [6] that will be investigated in the next section. The maximum amplification of energy increases with increasing λ^2/λ_{cr}^2, the oscillating behavior eventually tending to the exponential growth for $\lambda^2/\lambda_{cr}^2 \to 1$.

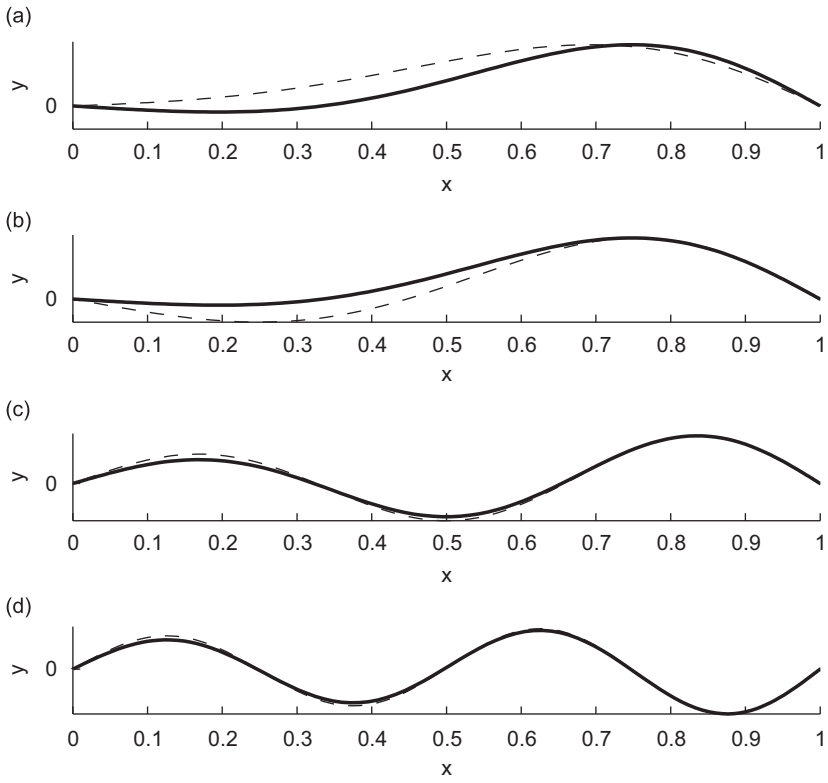

Fig. 2. Imaginary part of the first four eigenfunctions (displacement variable) for supersonic flow and no flow-induced damping: (a) 1st, (b) 2nd, (c) 3rd, (d) 4th eigenfunction. Values of λ^2/λ^2_{cr} are: 0.7 (dashed line), 1 (thick solid line), pinned–pinned case.

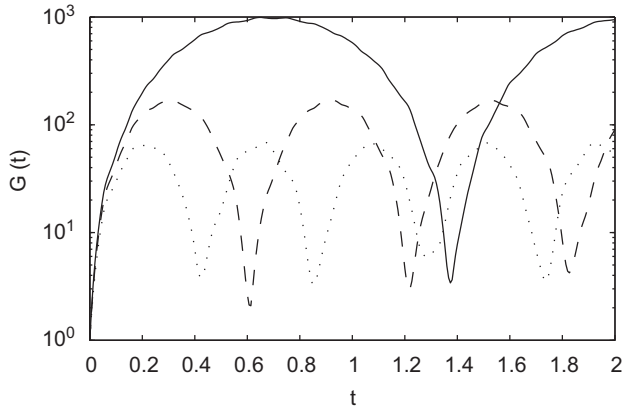

Fig. 3. Energy growth functions for supersonic flow and no-flow induced damping. Values of λ^2/λ^2_{cr} are: ··· 0.8, – – 0.9, — 0.98, pinned–pinned case.

A parallel analysis has been developed in order to directly simulate the dynamics of the panel, whose results are reported in Figs. 5 and 6 for $\lambda^2/\lambda^2_{cr} = 0.8$ and 0.98, respectively. In both cases the first eigenfunction of the *in vacuo* case, with unit amplitude and null initial velocity, has been considered as initial condition. Besides the instantaneous shape of the plate, Figs. 5(a) and 6(a), the evolution of the total, elastic potential and kinetic energies are monitored, Figs. 5(b) and 6(b), together with the term representing the energy exchange rate, $Q_e = -\int_0^1 p y_t \, dx$, between fluid and solid, Figs. 5(c) and 6(c). All energies are normalized with respect to the initial total value.

The maximum amplitude deformation (thick red line in both Figs. 5(a) and 6(a)) resembles the features of the almost coincident imaginary parts of the first pair of eigenfunctions. This is due to the fact that non-normality is practically confined in the subspace spanned by these two modes, hence the contribution to the norm of the solution given by the components of the initial condition in this subspace is dominant. Such a behavior is increasingly more evident as the critical condition is approached. Regarding the energy budget, Figs. 5(b) and 6(b) clearly depict that during the oscillatory

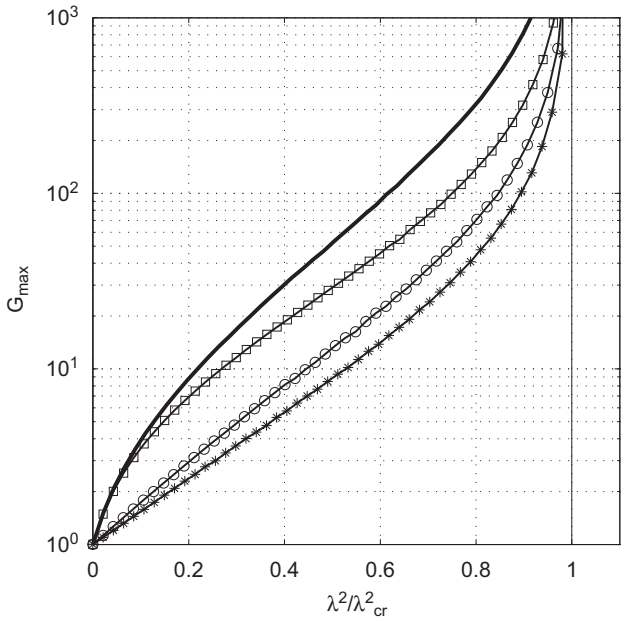

Fig. 4. Maximum value of optimal energy amplification vs λ^2/λ^2_{cr}. Symbols refer to steady supersonic flow and different boundary conditions: "*" C–C, "○" P–P, " □" C–F. Thick line refers to subsonic flow (Eq. (14)), clamped–free case.

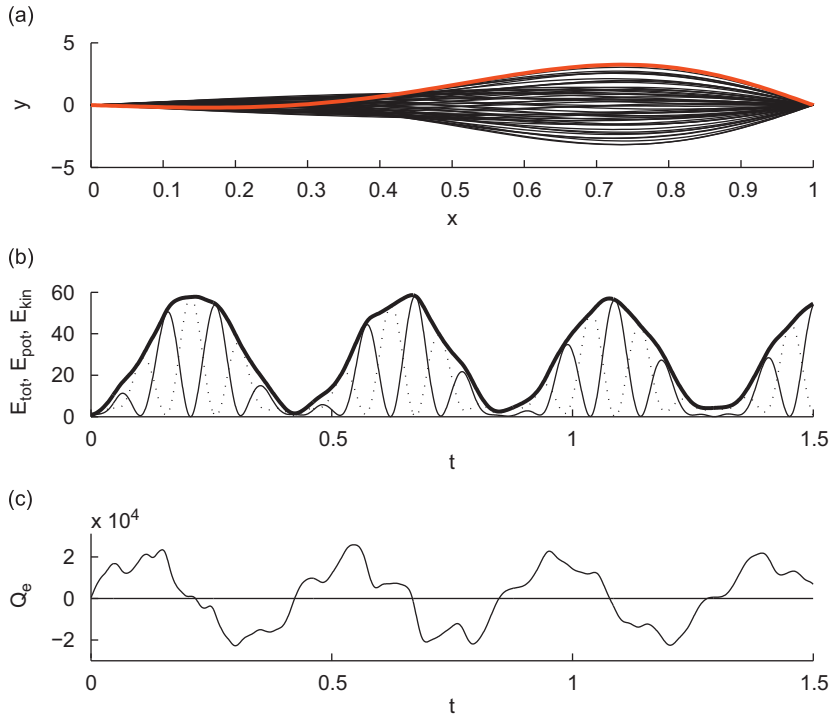

Fig. 5. Numerical simulation of Eq. (13) without aerodynamics damping for P–P case and $\lambda^2/\lambda^2_{cr} = 0.8$: (a) instantaneous deformation shapes; (b) kinetic energy (dotted line), potential energy (continuous line) and total energy (thick line); (c) energy exchange rate.

evolution of the total energy (thick line) there is a continuous conversion of kinetic energy (dotted line) into potential energy (continuous line) and vice versa, due to the high-frequency flapping dynamics of the plate. However, the total energy oscillates at a lower frequency and envelops the oscillations of potential and kinetic energies. The time evolution of the energy exchange rate verifies with accuracy the relation $Q_e = \mathrm{d}E_{\mathrm{tot}}/\mathrm{d}t$.

It should be explicitly noted that the initial condition chosen for the numerical simulations is not the optimal one. However, one may verify that imposing an initial static deformation coinciding with the first *in vacuo* eigenmode yields an

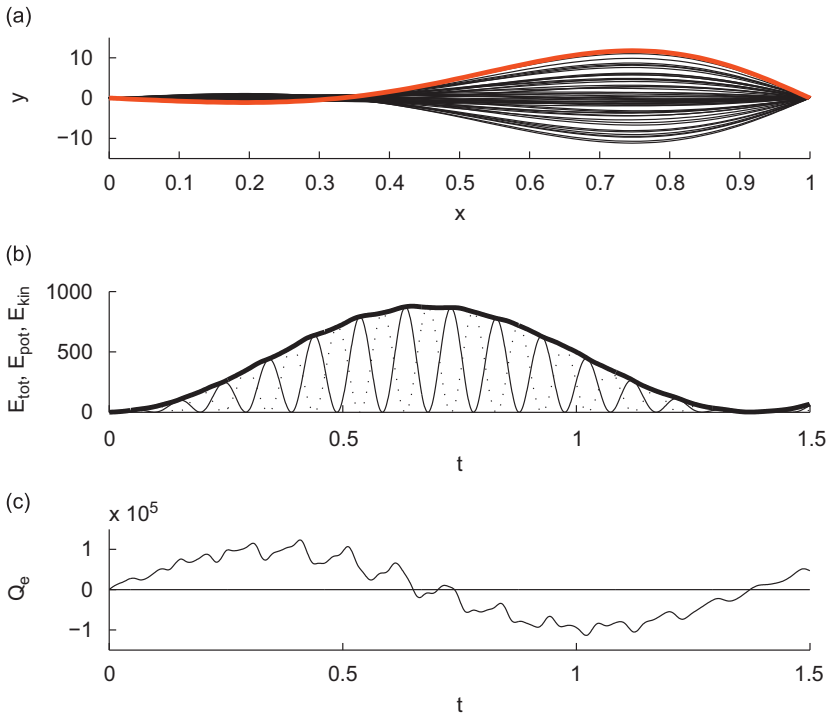

Fig. 6. Numerical simulation of Eq. (13) without aerodynamic damping for P–P case and $\lambda^2/\lambda_{cr}^2 = 0.98$: (a) instantaneous deformation shapes; (b) kinetic energy (dotted line), potential energy (continuous line) and total energy (thick line); (c) energy exchange rate.

energy evolution very close to the optimal one. Howell et al. [18] recently carried out similar direct numerical simulations (their initially imposed deformation was the second *in vacuo* eigenmode) and showed apparently analogous cycles of oscillation of energy for a clamped–free panel in subsonic flow. They deduced that the irreversible energy transfer between fluid and structure at critical conditions is the cause of the instability. Most importantly, Howell et al. [18] simulations refer to critical conditions in the presence of flow-induced damping, therefore the total energy evolution shows an oscillatory plateau, with a frequency coinciding with the flutter one.

In order to better elucidate this issue, we switched on the aerodynamic damping term of Eq. (13) and extended the considerations of Howell et al. [18] to subcritical conditions in the light of the non-modal theory. The morphology of the spectrum and the time evolution of the growth function modify, together with some characteristics of the periodic energy transfer between panel and fluid. Fig. 7(a) shows the path described by the imaginary parts of the first four eigenvalues as λ increases for various values of μ. The black line refers to the case of no damping, $\mu = 0$, while red and blue lines correspond to $\mu = 1$ and 5, respectively. Fig. 7(b) depicts the same information for the real parts. The unsteady contribution of the forcing pressure moves the instability onset toward higher values of λ and instability emerges not immediately after the collision of the first pair of eigenvalues. The optimal energy amplification oscillates in time with the same qualitative features as in the case of steady pressure field. However, the growth function $G(t)$ does not increase monotonically to infinity as λ approaches its critical value. On the contrary it reaches a plateau, afterward the panel loses its stability. This behavior is synthesized in Fig. 7(c) for various values of μ, including the no damping case $\mu = 0$. The full dot symbols represent the critical conditions which for the highest μ appear out of scale.

With much more detail Fig. 8 depicts the optimal energy amplification for $\mu = 0.5$ and various significant values of λ/λ_{cr} (now $\lambda_{cr} \simeq 20.26$). Besides the critical condition producing instability, the system exhibits another criticality at $\lambda/\lambda_{cr} \simeq 0.91$ when under stable conditions the first pair of eigenvalues collide. For $\lambda/\lambda_{cr} < 0.91$ the structure initially extracts energy from the fluid but it is able subsequently to release it through the usual low-frequency oscillations, the damping intensity determining the level of G_{max} and producing the asymptotic decay. After the eigenvalue splitting the structure can no longer balance the pressure forcing, in fact (e.g. $\lambda/\lambda_{cr} = 0.95$) the low-frequency oscillations disappear (the high-frequency ones only survive, corresponding to flutter frequency) and stability is guaranteed by the aerodynamic damping effect dissipating the rate of work done by the fluid. Note that the mean slope of $G(t)$ after the peak is negative. It is clearly evident that at critical conditions the rate of work done by the fluid is exactly dissipated by the damping effect, i.e. $dE_{tot}/dt = 0$ after the transient period. The typical oscillatory trends found by Howell et al. [18] looks like the case $\lambda/\lambda_{cr} = 1$. For $\lambda/\lambda_{cr} > 1$ the fluid rate of work is not shut off by dissipative effects and instability emerges.

The variation of G_{max} against μ is also shown in Fig. 7(d) for various λ/λ_{cr}. One should note that λ_{cr} depends in turn on μ.

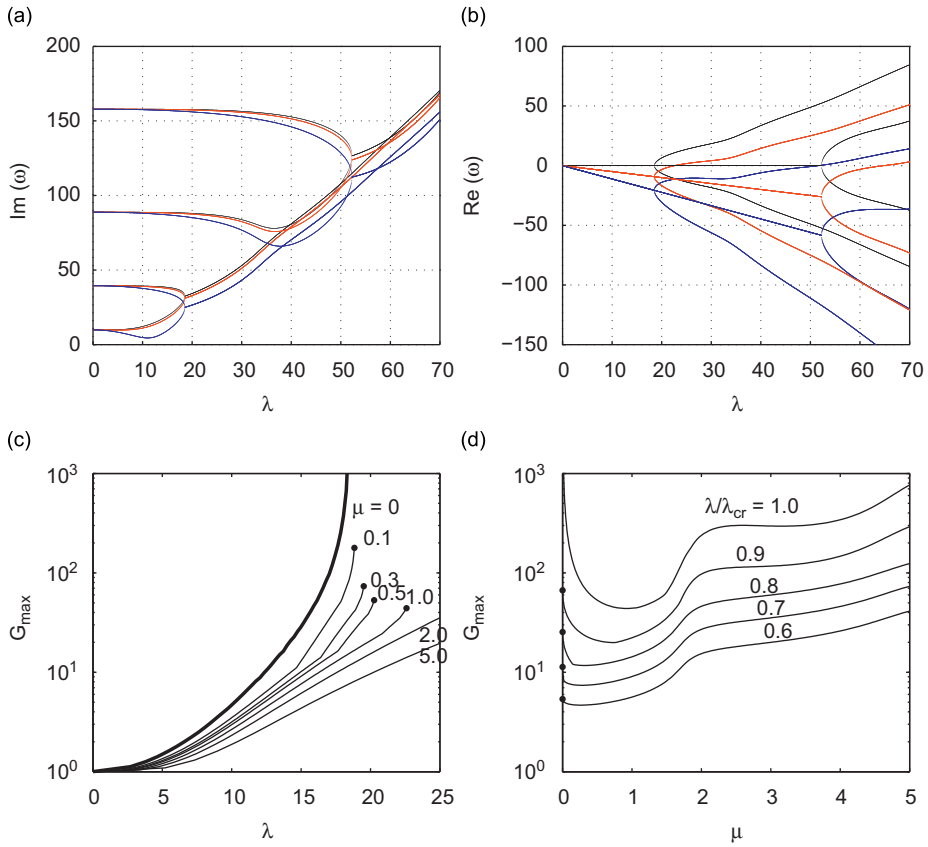

Fig. 7. Eigenvalue paths: (a) imaginary part and (b) real part; values of μ are: 0 (black line), 1 (red line), 5 (blue line). Maximum energy growths (c) and (d). Supersonic unsteady P–P cases. (For interpretation of the references to color in this figure legend, the reader is referred to the web version of this article.)

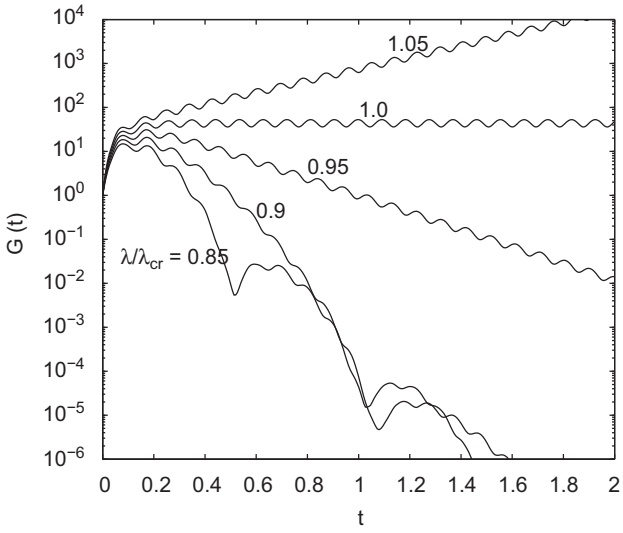

Fig. 8. Optimal growths for unsteady supersonic flow, $\mu = 0.5$.

4.2. *Subsonic flow: high-density flag*

The case of thin panel exposed to axial subsonic incompressible flow will be hereafter analyzed with reference to the simplified model developed by Argentina and Mahadevan [6] in which a quasi-steady approximation is made and the

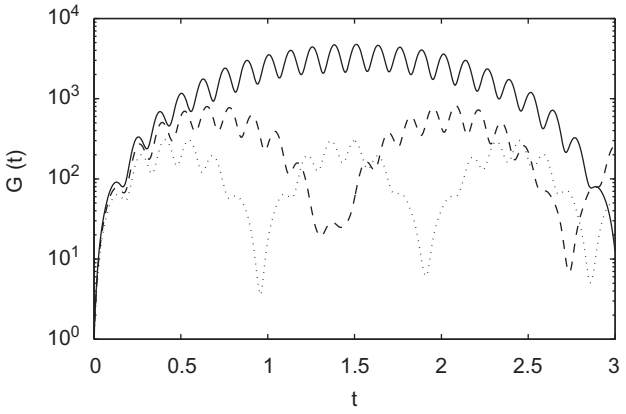

Fig. 9. Energy growth functions for subsonic flow model of [6] with C–F ends and $\mu \ll 1$. Values of λ^2/λ_{cr}^2 are: $\cdots$ 0.8, – – 0.9, — 0.98.

pressure field depends on the local deflection slope. This gives rise to flutter instability of coupled-mode type. In the subsequent section we will consider the potential model of non-circulatory flow of Kornecki et al. [3] in order to study the non-modal characteristics in the presence of non-local effects. Note that the simple models here considered lead to exact modal-coalescence instability. On the other hand, it is known that for more complex situations higher-order single-mode flutter instabilities may emerge, and the application of the non-modal analysis should be checked in future activity.

Following Argentina and Mahadevan [6] we consider here the limiting situation in which the parameter characterizing the added mass effect is supposed to be small ($\mu \ll 1$), while the scaled velocity is assumed to be large ($V \gg 1$) in such a way that the control parameter $\lambda = V\sqrt{\mu}$ remains finite. The physical situation under examination corresponds to a heavy flag in a fast flow. In this limit the vorticity is advected rapidly from the trailing edge so that one can use a steady approximation. The equation for the vertical displacement of the plate has the form:

$$\frac{\partial^2 y}{\partial t^2} = -\frac{\partial^4 y}{\partial x^4} - \lambda^2 \psi(x) \frac{\partial y}{\partial x} \tag{14}$$

where $\psi(x) = 2\sqrt{(1-x)/x}$. The boundary conditions here considered are of the type clamped–free, with the clamped end located at the trailing edge of the plate. The morphology of the spectrum is similar to that described for the panel in supersonic flow and the system loses stability through coupled-mode flutter. For the assigned clamped–free boundary conditions, in agreement with Argentina and Mahadevan [6] the critical value is $\lambda_{cr} \simeq 10.53$. Fig. 9, depicting the optimal energy amplification evolution, is particularly meaningful since, besides confirming all the characteristics already discussed in Section 4.1, shows clearly the influence of the flapping dynamics of the plate, which is responsible for the high-frequency oscillations. Such a behavior is exhibited also by the model of the clamped–free plate in supersonic flow (not shown) and hence it has to be associated to the peculiarity of the boundary conditions and not to the particular pressure model employed.

The occurrence of the high frequency oscillations is confirmed by the results of the numerical simulation, which are reported in Fig. 10 for $\lambda^2/\lambda_{cr}^2 = 0.9$. Again the simulation has been performed by considering as initial condition the first eigenfunction of the free oscillating plate *in vacuo* and the maximum amplitude deformation (red line in Fig. 10(a)) resembles the almost coincident imaginary parts of the first pair of eigenfunctions. The maximum growth of the normalized energy is as large as 800. All the physical comments previously made for the supersonic panel flutter applies to the present subsonic model, so that Fig. 10 is self-explaining. The values of G_{max} computed for various λ^2/λ_{cr}^2 have been already presented in Fig. 4.

4.3. Non-local subsonic pressure field

The influence of a non-local pressure field relative to an inviscid non-circulatory flow is now approached. We will refer here to the analytical model of Kornecki et al. [3] equipped with clamped–clamped end conditions. The governing equation (2) writes accordingly

$$\frac{\partial^2 y}{\partial t^2} = -\frac{\partial^4 y}{\partial x^4} + \frac{1}{\pi}\left\{\int_0^1 \left[\lambda^2 \frac{\partial^2 y}{\partial \xi^2} + 2\lambda\sqrt{\mu}\frac{\partial^2 y}{\partial \xi \partial t} + \mu \frac{\partial^2 y}{\partial t^2}\right] \ln|x-\xi|\, d\xi\right\} - d\frac{\partial y}{\partial t} \tag{15}$$

where the terms $\partial^2 y/\partial \xi^2$, $\partial^2 y/\partial \xi \partial t$, $\partial^2 y/\partial t^2$ represent the centrifugal, Coriolis and translatory accelerations of the fluid, respectively, and may be seen as effects of flow induced stiffness due to curvature, damping and additional inertia. The function $\ln|x-\xi|$ acts as a filter accounting for the non-local effects. The singularity of Eq. (15) is integrable and has been treated by means of a proper numerical procedure involving the "tanh" change of variables (cf. for example Boyd [23, p. 458]).

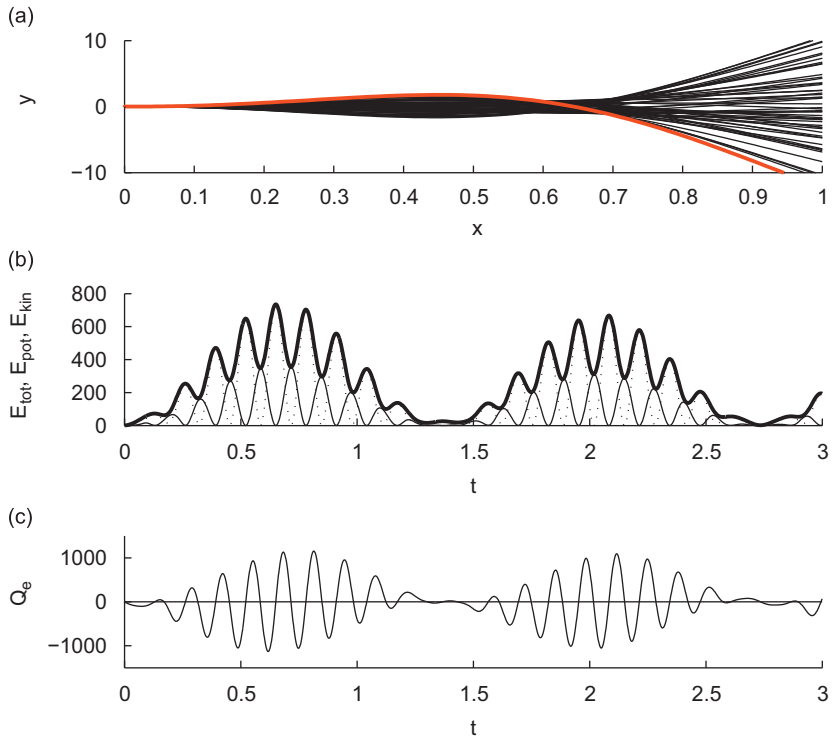

Fig. 10. Numerical simulation of Eq. (14) for $\lambda^2/\lambda_{cr}^2 = 0.9$ and C–F end conditions. Symbols are as for Fig. 5. (For interpretation of the references to color in this figure legend, the reader is referred to the web version of this article.)

First of all it has to be noticed that with Kornecki's model the plate typically loses its stability by divergence, for both clamped–clamped and pinned–pinned ends (the case clamped–free being of flutter-type). The operator is non-normal and oscillatory growths of energy due to disturbance amplification are computed. We found that the influence of the μ parameter is opposite to that observed for the supersonic model, since the growth peak G_{max} increases with increasing μ, as shown in Fig. 11(a). Fig. 11(b) depicts the weak influence of the dimensionless parameter of structural damping d for $\mu = 1$ and 10. The frequency of the oscillations against μ is decreasing due again to the added mass effect, as shown in Fig. 12 for undamped cases and $\lambda/\lambda_{cr} = 0.9$. G_{max} roughly scales like $(2+\mu)/2$, while the period T scales like $\sqrt{1+\mu}$.

Fig. 13 compares some $G(t)$ trends for undamped and damped configurations at incipient criticality ($\lambda/\lambda_{cr} = 0.9$) and at critical conditions ($\lambda/\lambda_{cr} = 1$). Damping of course reduces the energy growth, and G_{max} appears bounded at the instability onset in the presence of damping. Since the instability is achieved by divergence, here the period of global oscillation is related to the spacing between the (symmetric) imaginary parts of the first complex conjugate pair of eigenvalues.

The outputs of the direct simulations referring to undamped cases for $\mu = 10$ are reported in Figs. 14 and 15, the former when the instability onset is approaching, the latter at criticity, respectively. Since in the divergence case the high-frequency oscillations of the local transverse displacement disappear, the global oscillations of the energy growth function correspond directly to the transverse displacement oscillations of the panel. The energy exchanged with the fluid moves exclusively in potential energy and does not give rise to a continuous flowing of energy between potential and kinetic (as already observed in the flutter case). Note that in the present case the initial condition is given with a small amount of kinetic energy. In fact, Figs. 14(b) and 15(b) show that the kinetic energy is practically negligible as compared to the other energy forms.

Because of the absence of high-frequency oscillations the structure looks like a system without restoring forces since the structural stiffness is balanced by the aerodynamic stiffness. Here again the non-modal analysis gives a picture for the divergence onset as an instability which settles in via periodic transfers of energy of the panel from/to the fluid, illustrated in Figs. 14(c) and 15(c), with a period which becomes infinite at critical conditions.

4.4. Another interpretation of the global energy oscillations

The global oscillations of energy of the *optimal* amplifications may enclose another interesting reading-key of the modal-coalescence instabilities analyzed above. The starting point is the consideration that the period of low-frequency oscillations is strictly linked to the spacing between the imaginary parts of the coupling eigenvalues (typically the first two). Previous supersonic and subsonic models of pressure field demonstrated that this is a robust common characteristic.

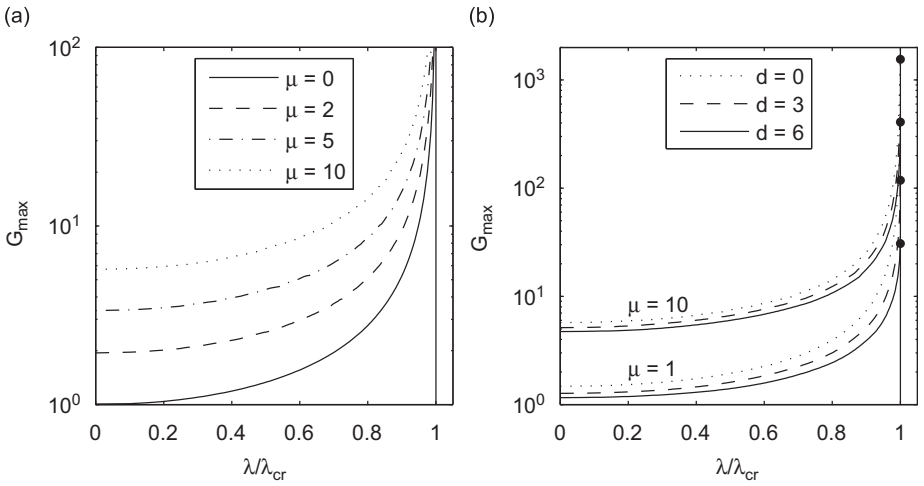

Fig. 11. Maximum energy amplification for subsonic Kornecki's model, with C–C ends: (a) undamped cases for various μ and (b) damped cases for $\mu = 1$ and 10.

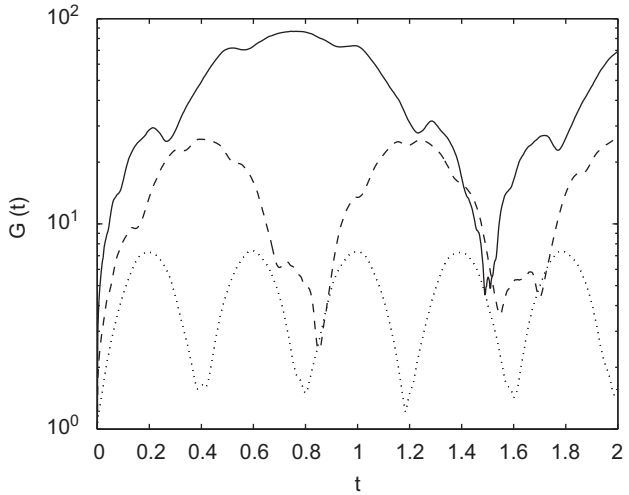

Fig. 12. *Optimal* growth evolution for the Kornecki's model with C–C ends for $\lambda/\lambda_{cr} = 0.9$ and no structural damping. Values of μ are: ··· 1, – – 10, — 40.

This occurrence has a very strong analogy with the beats phenomenon verifying in the dynamics of forced damped mass-spring systems governed by the equation

$$\ddot{x} + d\dot{x} + \omega_0^2 x = F\sin\omega_f t \tag{16}$$

A typical steady energy evolution exhibits a high-frequency conversion between kinetic and potential energy enveloped by a low-frequency oscillation of the total energy, which reproduces exactly for instance the trend of Fig. 10(b) for undamped situation, and those of Fig. 8 for damped situation. The high-frequency is given by the natural pulsation ω_0 of the oscillator, while the low-frequency is determined by the difference between the natural and forcing frequencies $\omega_0 - \omega_f$, giving rise to beats. Note that the frequency of the oscillations of energy is twice that of the displacement variable x because symmetric displacements have the same content of energy.

A similar behavior is exhibited by the two coupled oscillators of Eq. (7) even in the presence of damping, as shown by Schmid and de Langre [19]. It is clear that in this model the forcing term of an oscillator is constituted by the oscillating evolution of the other one. The difference with respect to the externally forced system is that the global frequency of the enveloping oscillations is here given by the difference between the two natural frequencies, depending on the coupling parameter a. Indeed, this was already found by Schmid and de Langre [19], although they did not relate the global energy oscillations to the beats occurrence.

Our differential models of previous sections exhibit a countable set of infinite natural vibration modes coupled to each other by the flow-induced pressure term. Since the non-normality is practically restricted (at least for the cases here

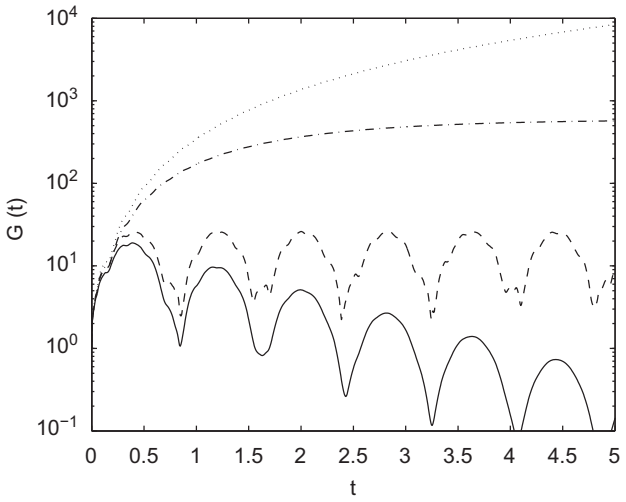

Fig. 13. *Optimal* growth evolution for the Kornecki's model with C–C ends. Continuous line $\mu = 10$, $d = 5$, $\lambda/\lambda_{cr} = 0.9$; dashed line $\mu = 10$, $d = 0$, $\lambda/\lambda_{cr} = 0.9$; dashed-dotted line $\mu = 10$, $d = 5$, $\lambda/\lambda_{cr} = 1$; dotted line $\mu = 10$, $d = 0$, $\lambda/\lambda_{cr} = 1$.

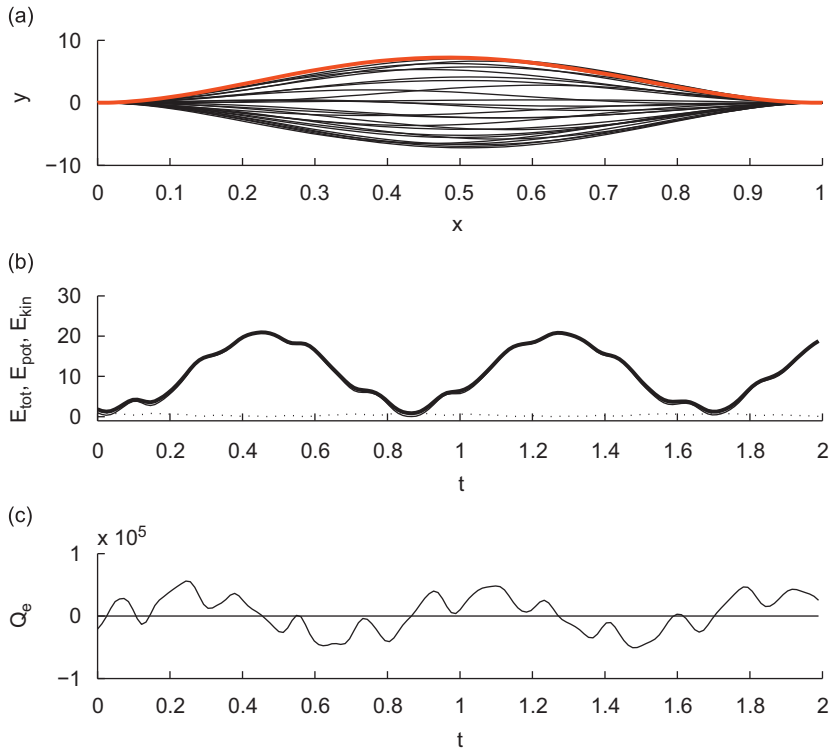

Fig. 14. Numerical simulation of Eq. (15) for $\lambda/\lambda_{cr} = 0.9$, $\mu = 10$, $d = 0$ and C–C end conditions. Symbols are as for Fig. 5.

analyzed) to the first pair of eigenvalues, one can interpret the global subcritical oscillations of energy as the result of a resonance between two coupled oscillators (the flow-dependent eigenvalues). Furthermore, in the case of divergence, since the actual stiffness vanishes, one eigenvalue vanishes as well and the energy resonance frequency is expected to be twice the second eigenmode, as occurs for the Kornecki's model.

4.5. The pipe conveying a fluid

In Section 2 it has been observed that Eq. (1) is relevant for a class of problems wider than those strictly related to the panel flutter/divergence, as it describes, for instance, the small lateral motion of a pipe conveying a fluid. An exhaustive

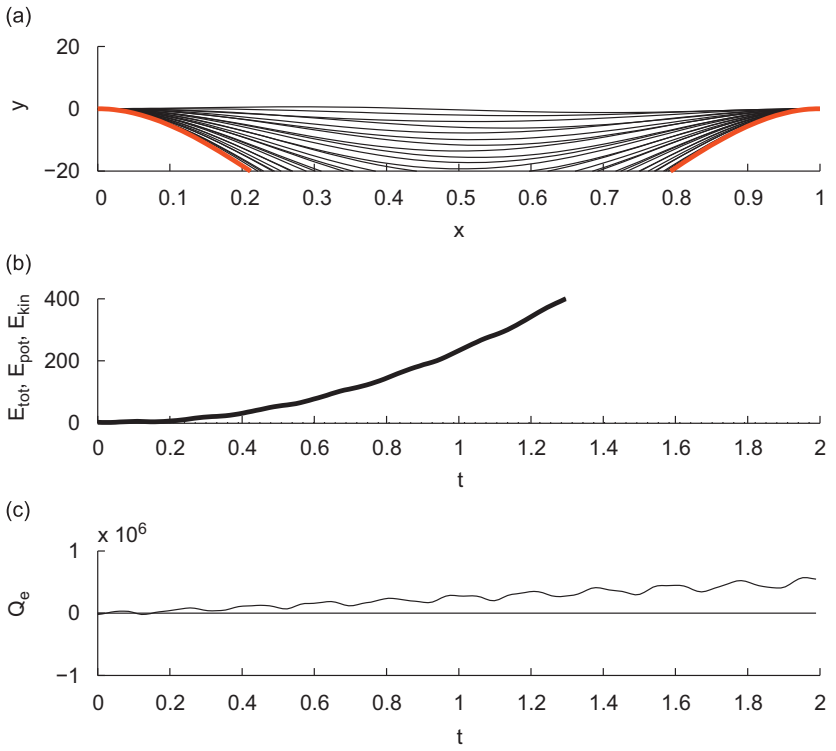

Fig. 15. Numerical simulation of Eq. (15) for $\lambda/\lambda_{cr}=1$, $\mu=10$, $d=0$ and C–C end conditions. Symbols are as for Fig. 5.

review of the investigation methodologies and physical considerations about the problem can be found in Paidöussis [1] and de Langre et al. [28]. A fluid-conveying pipe represents an occurrence of fluid–structure interaction where the system loses stability by flutter or divergence in a variety of manners, depending on the imposed boundary conditions. For fixed pipe ends the system is conservative, whilst the cantilevered case is not conservative due to the influence of flow induced damping effects.

If gravity, structural damping, externally imposed tension and pressurization effects are neglected, the equation of motion of the pipe takes the form

$$(M+m)\frac{\partial^2 Y}{\partial \tau^2}=-EI\frac{\partial^4 Y}{\partial X^4}-2MU\frac{\partial^2 Y}{\partial X\partial \tau}-MU^2\frac{\partial^2 Y}{\partial X^2} \tag{17}$$

where M is the mass of fluid per unit length, flowing with a steady velocity U, m is the mass of the pipe per unit length and EI is the flexural rigidity of the pipe. The term $M\partial^2 Y/\partial\tau^2$ is an added mass effect, the second spatial derivative term is associated to centrifugal forces in the fluid (and is usually termed aerodynamic stiffness), and the mixed derivative models the Coriolis effects (aerodynamic damping). Note that Eq. (17) can be derived from Eq. (1) when the forcing pressure is modeled as

$$\Delta P=M\left(\frac{\partial}{\partial \tau}+U\frac{\partial}{\partial X}\right)^2 Y \tag{18}$$

which coincides with a classic result of Lighthill [29] presented in a historical note on the slender fish swimming. Thus, as noted by Triantafyllou [30], Eq. (17) governs the dynamics of both cylinders in axial flow and conveying-fluid pipes.

In this last case the added mass is ρA, A being the cross sectional area of the pipe. Eq. (17) can be conveniently put in the following non-dimensional form

$$\frac{\partial^2 y}{\partial t^2}+\frac{\partial^4 y}{\partial x^4}+2\sqrt{\beta}u\frac{\partial^2 y}{\partial x\partial t}+u^2\frac{\partial^2 y}{\partial x^2}=0 \tag{19}$$

where non-dimensional parameters $\beta=M/(M+m)$ and $u=UL\sqrt{M/EI}$ have already been introduced in Section 2. The boundary conditions usually considered for this equation are both of fixed type (clamped–clamped or pinned–pinned) and cantilevered type (clamped–free).

For fixed type boundary conditions the system firstly loses stability via a couple-mode divergence of its first mode at a critical value u_{cr}, which is independently of β. Values of u_{cr} for the cases of pinned–pinned and clamped–clamped boundary conditions are $u_{cr}=\pi$ and $u_{cr}=2\pi$, respectively.

Our analysis shows that, before divergence instability the system becomes increasingly non-normal as the critical conditions are approached, although the overall level of non-normality is lower with respect to the previous cases, as already noted by Schmid and de Langre [19] for their simplified model. The growth function again reveals that the pipe is able to extract and release energy from the fluid in periodic cycles, in such a way that the energy exchanged in one period is globally zero (the system is conservative). The critical conditions being of divergence type, the oscillations of the *optimal* energy growth correspond exactly to the transverse displacement oscillations of the pipe and exchanged energy moves exclusively in potential energy, the structural stiffness being balanced by the flow induced stiffness. The instability settles in through periodic extractions and releases of energy of the pipe from the fluid, the period tending to infinite at critical conditions. Quantitative results are not presented herein because they are quite similar to the ones discussed for the Kornecki's model.

More interesting is the analysis of the cantilevered pipe, which presents a quite different situation. As analyzed in a great detail by Paidöussis [1], the topology of the spectrum before instability is generally more complex because the system is damped by the effects of the Coriolis force, which, unlike the case of fixed ends, is able to perform work. A similar occurrence has been observed for the supersonic panel model when the unsteady term of pressure has been taken into account within the *piston theory* approximation.

Fig. 16 depicts the spectrum computed for the typical situation of $u/u_{cr} = 0.9$ and $\beta = 0.5$, the critical value of u being $u_{cr} \simeq 9.32$. Here the first pair of eigenvalues experiences first two collisions followed by splitting before the third mode ultimately becomes unstable traversing the real axis. As fully described by Paidöussis [1], other modes can become

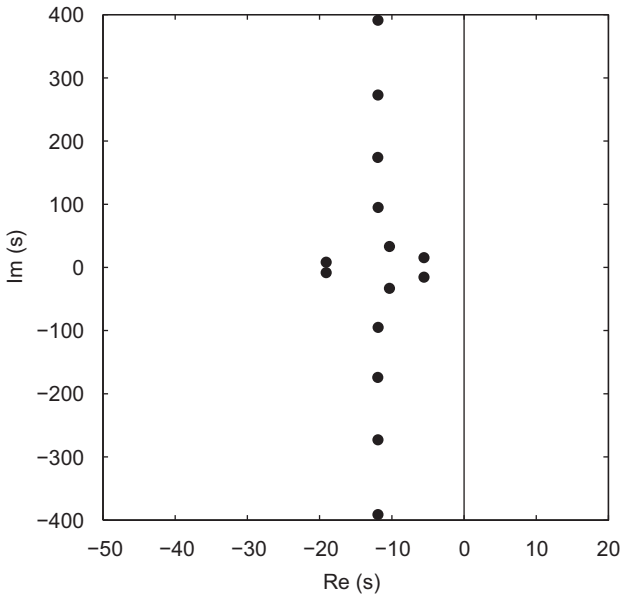

Fig. 16. Spectrum for the pipe-conveying fluid model, C–F ends. $u/u_{cr} = 0.9$, $\beta = 0.5$.

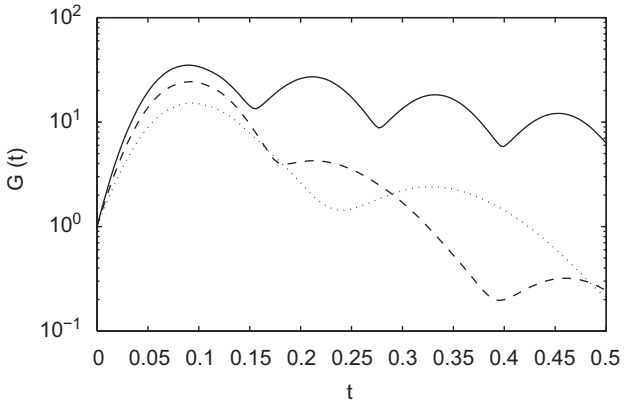

Fig. 17. Growth functions for the pipe-conveying fluid model, C–F ends. Values of u/u_{cr} are: $\cdots$ 0.8, – – 0.9, — 0.98. $\beta = 0.5$.

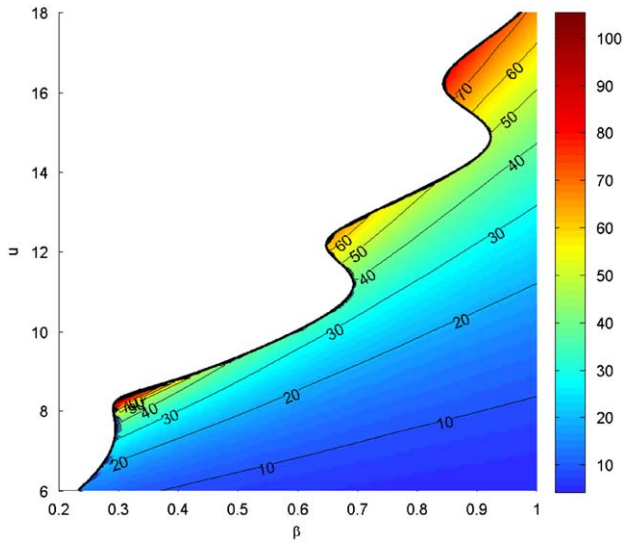

Fig. 18. Iso-contour G_{max} curves for the pipe conveying fluid model with C–F ends. White region is the modal unstable region.

unstable at different values of β and an interesting re-stabilization phenomenon can also occur at higher values of u for suitable values of β.

As regards non-normal features of the system, the general trend of increasing non-normality degree with increasing the scaled velocity u (at fixed β) is confirmed. Such a behavior is enhanced by each further collision, although the growth levels of energy remain in general lower than the ones achieved in the other cases considered before. Selected time trends of the growth function are reported in Fig. 17 where, after the initial increase, a characteristic decrease and oscillating behavior is clearly evident, recalling the finding of supersonic cases illustrated in Fig. 8.

The subsequent Fig. 18 shows a map in the plane $u-\beta$ of the computed values of G_{max}. The white region above the classical S-shaped marginal curve denotes asymptotic instability, whereas below it, where the pipe is asymptotically stable, significant transient growths of the energy are achieved. While for some fixed β values the eigenvalues analysis predicts alternating stable/unstable behaviors as the velocity parameter u is increased, the values of G_{max} continuously grow within the asymptotically stable region, except the interval of u where the system is unstable.

5. Final discussion and conclusions

A detailed theoretical study of the dynamics of typical fluid–structure interactions (involving thin plates and pipes conveying a fluid) in subcritical conditions has been conducted by making use of both typical methodologies of investigation of the linear non-modal operator theory and direct numerical simulations. To the knowledge of the present authors this is the first time that non-modal characteristics of the equations modeling phenomena of fluid–structure interaction are investigated, although we used here simple models of flow-induced pressure fields leading generally to modal-coalescence instability.

The *optimal* energy amplifications, here defined *global* because they refer to the entire structure as a whole, for all the cases examined exhibit low-frequency temporal oscillations which correspond physically to the continuous extraction/release of energy from/to the fluid. When any effect of damping is neglected the energy growth peak increases with increasing the intensity of the interaction, i.e. the scaled flow velocity, and eventually tends to infinity as the critical condition of instability is approached (resonance). In the presence of damping the *global* behavior shows similar features but in subcritical states the evolution of the energy amplification is asymptotically damped and attains a constant plateau at instability onset. Small-amplitude high-frequency oscillations may be also present, due to the actual (i.e. combined structural and aerodynamic) stiffness term.

The direct numerical simulations confirm this scenario, although one has to remember that they solve a specific initial value problem whilst the non-modal approach determines the greatest amplification of energy for all initial perturbations. It is found that the first static *in vacuo* eigenmode approximates very closely the *optimal* initial condition, and the maximum amplitude deformations are enveloped by the coinciding first and second eigenfunctions when critical conditions are approached.

We observed that the low-frequency of *global* oscillations is always related to the spacing of the imaginary parts of the coupling eigenvalues, which on the other hand represent essentially the non-normal part of the spectrum. This perhaps surprising finding may suggest that the periodic transfers of energy between fluid and structure along the route to the instability can be predicted by a simple model of damped forced vibrations, the beating frequency being given by the

distance between the two non-normal coupling eigenvalues. Peaks of *global* energy correspond to flow-induced beats. When the instability occurs by divergence, in particular, the actual stiffness of the structure vanishes and the high-frequency oscillations disappear; nonetheless the low-frequency oscillations (in this case the energy ones are directly linked to the transverse displacement ones) persist, the frequency being twice the imaginary part of the second eigenvalue.

It has to be stressed once again that our major findings have been obtained with simple pressure models employed in order to treat in a feasible way the rather wide cases of fluid–structure studied. The related instability is essentially of modal-coalescence type. However, we believe that most of the effects discussed in the paper have a strong survival chance in more complete flow dynamics modeling, at least at high Reynolds numbers, and recommend extending the investigation by making use of full Navier–Stokes equations. On the other hand, if we observe the problem from the fluid view-point the interaction flow-structure leads to fluid dynamics fields (e.g. open boundary layer flow or confined channel flow) including effects of compliant walls. It is already known that for the standard case of rigid boundary the Orr–Sommerfeld operator is non-normal and an asymptotically stable flow may exhibit large transient growths of energy that are eventually shut off by viscous effects. Low-frequency oscillations are not present because of the absence of reaction terms (rigid wall and incompressible flow). When the walls are compliant the reaction terms can produce low-frequency oscillations of fluid energy, as recently observed by Hœpffner et al. [31]. Of course, the presence or the absence of reaction effect depends on its relative magnitude with respect to other effects.

Acknowledgments

The authors wish to greatly thank the subject editor L. Huang and the anonymous third reviewer for the valuable issues raised during the revision of the manuscript stimulating the production of additional results and a clearer and in-depth exposition of the matter.

References

[1] M.P. Païdoussis, *Fluid–Structure Interactions. Slender Structures and Axial Flow*, Vol. 1, Elsevier Academic Press, London, 2004.
[2] M.P. Païdoussis, *Fluid–Structure Interactions. Slender Structures and Axial Flow*, Vol. 2, Elsevier Academic Press, London, 2004.
[3] A. Kornecki, E.H. Dowell, J. O'Brien, On the aeroelastic instability of two-dimensional panels in uniform incompressible flow, *Journal of Sound and Vibration* 47 (1976) 163–178.
[4] L. Huang, Flutter of cantilevered plates in axial flow, *Journal of Fluids and Structures* 9 (1995) 127–147.
[5] Y. Watanabe, K. Isogai, S. Suzuki, M. Sugihara, A theoretical study of paper flutter, *Journal of Fluids and Structures* 16 (2002) 543–560.
[6] M. Argentina, L. Mahadevan, Fluid-flow-induced flutter of a flag, *Proceedings of the National Academy of Sciences* 102 (6) (2005) 1829–1834.
[7] N. Yamaguchi, K. Yokota, Y. Tsujimoto, Flutter limits and behaviors of a flexible thin sheet in high-speed flow—I: analytical method for prediction of the sheet behavior, *Journal of Fluids Engineering* 122 (1) (2000) 65–73.
[8] D.M. Tang, H. Yamamoto, E.H. Dowell, Flutter and limit cycle oscillations of two-dimensional panels in three-dimensional axial flow, *Journal of Fluids and Structures* 17 (2003) 225–242.
[9] L. Tang, M.P. Païdoussis, On the instability and the post-critical behaviour of two-dimensional cantilevered flexible plates, *Journal of Sound and Vibration* 305 (2007) 97–115.
[10] E.H. Dowell, H.M. Voss, Theoretical and experimental panel flutter studies in the Mach number range 1.0 to 5.0, *AIAA Journal* 3 (12) (1965) 2292–2304.
[11] J. Dugundji, Theoretical considerations of panel flutter at high supersonic Mach numbers, *AIAA Journal* 4 (6) (1966) 1257–1266.
[12] E.H. Dowell, *Aeroelasticity of Plates and Shells*, Noordhoff International Publishing, Leyden, 1975.
[13] M.P. Païdoussis, The canonical problem of the fluid-conveying pipe and radiation of the knowledge gained to other dynamics problems in Applied Mechanics, *Journal of Sound and Vibration* 310 (2008) 462–492.
[14] M. Shelley, N. Vandenberghe, J. Zhang, Heavy flags undergo spontaneous oscillations in flowing water, *Physical Review Letters* 94 (2005) 094302.
[15] J. Zhang, S. Childress, A. Libchaber, M. Shelley, Flexible filaments in a flowing soap film as a model for one-dimensional flags in a two-dimensional wind, *Nature* 408 (2000) 835–839.
[16] I.D. Abrahams, G.R. Wickham, On transient oscillations of plates in moving fluids, *Wave Motion* 33 (2001) 7–23.
[17] M.W. Pitman, A.D. Lucey, On the direct determination of the eigenmodes of finite flow-structure systems, *Proceedings of the Royal Society A* 465 (2009) 257–281.
[18] R.H. Howell, A.D. Lucey, P.W. Carpenter, M.W. Pitman, Interaction between a cantilevered-free flexible plate and an ideal flow, *Journal of Fluid and Structures* 25 (2009) 544–566.
[19] P.J. Schmid, E. de Langre, Transient growth before coupled-mode flutter, *Journal of Applied Mechanics* 70 (6) (2003) 894–901.
[20] P. Hémon, E. de Langre, P. Schmid, Experimental evidence of transient growth of energy before airfoil flutter, *Journal of Fluids and Structures* 22 (2006) 391–400.
[21] G. Coppola, L. de Luca, On transient growth oscillations in linear models, *Physics of Fluids* 18 (2006) 078104.
[22] L.N. Trefethen, *Spectral Methods in MATLAB*, SIAM, Philadelphia, PA, 2000.
[23] J.P. Boyd, *Chebyshev and Fourier Spectral Methods*, second ed., Springer, Berlin, 2001.
[24] J.A.C. Weideman, S.C. Reddy, A MATLAB differentiation matrix suite, *ACM Transactions on Mathematical Software* 26 (4) (2000) 465.
[25] P.J. Schmid, D.S. Henningson, *Stability and Transition in Shear Flows*, Springer, Berlin, 2001.
[26] L.N. Trefethen, M. Embree, *Spectra and Pseudospectra: The Behavior of Nonnormal Matrices and Operators*, Princeton University Press, Princeton, NJ, 2005.
[27] S.C. Reddy, D.S. Henningson, Energy growth in viscous channel flows, *Journal of Fluid Mechanics* 252 (1993) 209–238.
[28] E. de Langre, M.P. Païdoussis, O. Doaré, Y. Modarres-Sadeghi, Flutter of long flexible cylinders in axial flow, *Journal of Fluid Mechanics* 571 (2007) 371–389.
[29] M.J. Lighthill, Note on the swimming of slender fish, *Journal of Fluid Mechanics* 9 (1960) 305–317.
[30] G.S. Triantafyllou, Physical condition for absolute instability in inviscid hydroelastic coupling, *Physics of Fluids A* 4 (1992) 544–552.
[31] J. Hœpffner, A. Bottaro, J. Favier, Mechanisms of non-modal energy amplification in channel flow between compliant walls, *Journal of Fluid Mechanics* (2009), in press. 〈http://www.jfm.damtp.cam.ac.uk/In_Press.html〉.